Calculation of charge-changing cross-sections of ions or atoms colliding with fast ions using the classical trajectory method ☆

I.D. Kaganovich *, Ariel Shnidman, Harrison Mebane, R.C. Davidson

Plasma Physics Laboratory, Princeton University, Princeton, NJ 08543, USA

ARTICLE INFO

ABSTRACT

Evaluation of ion–atom charge-changing cross-sections is needed for many accelerator applications. A Classical Trajectory Monte Carlo (CTMC) simulation has been used to calculate ionization and charge-exchange cross-sections. For benchmarking purposes, an extensive study has been performed for the simple case of hydrogen and helium targets in collisions with various ions. Despite the fact that the simulation only accounts for classical mechanics, the calculations are comparable to experimental results for projectile velocities in the region corresponding to the vicinity of the maximum cross-section. The shortcomings of the CTMC method for multielectron target atoms are discussed.

1. Introduction

Ion–atom ionizing collisions are of considerable interest in atomic physics [1] and play an important role in many applications such as heavy ion inertial fusion [2], collisional and radioactive processes in the Earth's upper atmosphere [3], atomic spectroscopy, ion stopping in matter, and ion-beam lifetimes in accelerators [4]. For example, electron clouds can form inside the accelerator due to residual gas ionization and cause two-stream instabilities [5]. The formation of electron clouds and the beam loss due to stripping can cause severe limitations on parameters of the vacuum system for the heavy ion synchrotron SIS18 at GSI operating with heavy ion beams [6]. Beam interaction with the remaining background gas and gas desorbing from the walls can limit the charge bunch intensity at the Relativistic Heavy Ion Collider (RHIC) [7], and is also a concern for the Large Hadron Collider (LHC) [8]. Similarly, it is of great concern for the positron damping ring of the International Linear Collider (ILC) [9], as well as for other high current, high-intensity accelerators and ion-beam injectors.

The recent resurgence of interest in charged particle beam transport in background plasma is brought about by the recognition that plasma can be used as a magnetic lens [10]. To estimate the ionization and stripping rates of fast ions propagating through gas or plasma, the values of ion–atom ionization cross-sections are necessary. In contrast to the electron and proton ionization cross-sections, where experimental data or theoretical calculations exist for practically any ion or atom, the knowledge of ionization cross-sections by fast complex ions and atoms is far from complete. For this reason the US Heavy Ion Fusion Science Virtual National Laboratory has initiated measurements of cross-sections in a series of experiments at GSI [11–13] and the Texas A&M synchrotron [14,15]. When experimental data and theoretical calculations are not available, approximate formulae are needed; therefore, the scaling of cross-sections with energy and target or projectile nucleus charge has been developed to approximate these values of cross-sections over a broad range of energies and charge states [1,12,16].

For the interaction of complex projectile and target atoms or ions, Classical Trajectory Monte Carlo (CTMC) simulations can be utilized [17]. Classical mechanics approaches are typically simple to apply and yield fairly reliable total cross-sections for collision processes at intermediate energies [18]. The CTMC was originally developed by Abrines and Percival [19], and has been used to investigate various collisional processes. The CTMC method consists of computing the electron trajectory in an atom when another ion or atom is passing by at a certain impact parameter. The cross-section is obtained from the rate of occurrence of the outcome of the collision. The electron can remain close to one of the nuclei or it can move far away from both of them. If the electrons remain close to the target or projectile nuclei, and the electron kinetic energy is smaller than the attractive potential to the nucleus, the electron is assumed to be trapped by target or projectile nuclei. If the electron is trapped by the target nucleus, no ionization or charge-exchange event occurs, but if the electron is trapped by the projectile nucleus, the charge-exchange event occurs. Conversely, if the electron moves away from the target and projectile nuclei, ionization takes place. The atomic potentials can be determined using either Thomas–Fermi theory or Hartree–Fock theory, which include orbital effects. The Hartree–Fock atomic wave equations are solved using Slater determinants [20].

The calculations show that the Thomas–Fermi model describes well most of the potential, but does not describe accurately the ion potential at the outer edge of an ion even for relatively high charge Z ($Z > 19$). The difference in atomic potentials can give an error of about 20% compared with the calculations utilizing the more accurate Slater model [20]. Therefore, in the following, we use primarily the latter model for the ion and atom potentials.

Though frequently used, we have not found a detailed study of the validity of the CTMC method. The validity trajectory approximation has been studied by comparing the results of simulations with available experimental data and the full quantum-mechanical calculations in Ref. [1]. Additionally, a theoretical criterion has been developed for the validity of the classical trajectory approximation in Ref. [21]. The range of validity of the Born approximation and the quasi-classical of the classical approximation can be estimated by evaluating the action $S(\rho, vt) = \int_{-\infty}^{\infty} \Phi_p[r(\rho, vt)]dt$ along the trajectory $r(\rho, vt) = [\rho^2 + (vt)^2]^{1/2}$. Here, $\Phi_p(r)$ is the projectile atomic potential, ρ is the impact parameter, and v is the projectile velocity. When $S(\rho, v) > \hbar$, we can apply classical mechanics [1], whereas the Born approximation fails. At higher velocities when $S(\rho, v) < \hbar$, quantum-mechanical effects become more significant and the CTMC results agree less with the experimental values of cross-sections, whereas the Born approximation is valid. Also at very low velocities, $S(\rho, v) \gg \hbar$, the probability of charge-exchange transitions in classical mechanics may be significantly less than that due to classically forbidden transitions, which can be described in quantum mechanics using quasi-classical approximations, see e.g., Ref. [1] for more details. Therefore, the CTMC method can be generally applied in the narrow range $S(\rho, v) \sim \hbar$. To further investigate the region of validity, an extensive study has been performed for the simple case of hydrogen and helium targets in collisions with various ions.

2. Description of the CTMC method

Application of the CTMC method consists of computing of the electron trajectory in an atom when another ion or atom is passing by at a certain impact parameter. For calculating the total cross-sections, it is only necessary to determine the outcome of the collision, i.e., the electron velocity and distances to the target and projectile nuclei at large enough times, when one of the distances is sufficiently large. There are three possible outcomes: the electron remains close to one of the nuclei, or it moves far away from both of them. If the electron kinetic energy (in the appropriate reference frame) is smaller than the attractive potential of the target or projectile, the electron is assumed to be trapped by the nucleus. If the electron remains near the target, no ionization or charge-exchange events have occurred. If the electron is trapped by the projectile nucleus, the exchange event has occurred. If none of these events has happened, ionization takes place. The results have to be averaged over all possible initial electron positions and impact parameters.

The result of the calculation should not depend on the set of initial conditions for the electron trajectories. To properly initialize the calculation, the initial set of electron positions should sample a steady-state distribution in phase space of an atom or ion without the projectile present. In order to have a steady-state distribution, the Electron Velocity Distribution Function (EVDF) should be a function of constants of the motion: the total energy, which is equal to the electron orbital binding energy $E_{ln} = -I_{nl}$, where I_{nl} is the ionization potential, and the total orbital momentum L. For the best correspondence between quantum mechanics and classical mechanics, we choose $L = l + 0.5$ [22], where l is the quantum number characterizing the orbital

momentum. In classical mechanics, the EVDF of an electron orbital n,l is given by the microcanonical ensemble distribution in the phase space volume $d\Gamma = d^3\mathbf{r}\,d^3\mathbf{v}$, i.e.,

$$f_{n,l}(\mathbf{v}_e, \mathbf{r})d\Gamma = C_{n,l}\delta\left[\frac{mv_e^2}{2} + \Phi_{n,l}(r) - E_{nl}\right]\delta(L - |\mathbf{v}_e \times \mathbf{r}|)d^3\mathbf{r}\,d^3\mathbf{v}. \quad (1)$$

Here $\Phi_{n,l}(r)$ is the atomic potential describing the interaction of the atomic electron with the nucleus and the rest of the electrons, and $C_{n,l}$ is a normalization constant. In Eq. (1), it was assumed that the direction of angular momentum is not specified and has been averaged over all possible directions. We use spherical coordinates $d^3\mathbf{r} = r^2\sin\theta\,dr\,d\theta\,d\phi$. The velocity vector can be split into two components: one is directed along the radius vector $\mathbf{v}_r$, and the rotational velocity, $\mathbf{v}_\beta$, is rotated in the plane perpendicular to $\mathbf{v}_r$ by an angle α (see Fig. 1). For a spherically symmetric model of an atom, the rotation velocity, v_β, is determined by angular momentum conservation $L = v_\beta r$; and the radial electron velocity is determined from energy conservation

$$v_r^2 + (L/r)^2 = -2I_{n,l} - 2\Phi_{n,l}(r). \quad (2)$$

Integrating the EVDF over phase space $d^3\mathbf{r}\,d^3\mathbf{v}$ is straightforward in cylindrical coordinates in velocity space $d^3\mathbf{v} = dv_r\,d\alpha\,v_\beta\,dv_\beta$. Substituting into Eq. (1) then gives

$$f_{n,l}(\mathbf{v}_e, \mathbf{r})d\Gamma = C_{n,l}\delta\left[\frac{mv_e^2}{2} + \Phi_{n,l}(r) - E_{nl}\right]\delta(L - v_\beta r)\,d^3\mathbf{r}\,d\alpha\,dv_r\,v_\beta\,dv_\beta$$
$$= \frac{LC_{n,l}}{m}\frac{dr}{v_r(r,l)}\sin\theta\,d\theta\,d\phi\,d\alpha \quad (3)$$

where the radial velocity $v_r(r,l)$ is given by Eq. (2).

To integrate over the initial positions of an electron in an atom, we can use a Monte Carlo stochastic method where the initial conditions are chosen randomly. In the general case, weights in the probability calculation have to be used before summing up the outcomes for cross-section calculations. This is because, if one picks values of the electron velocity and radius randomly, this does not correspond to a uniform distribution of points on a surface of the sphere in phase space, i.e., to a microcanonical ensemble. Therefore, instead of initializing the variable radius, we use the phase of motion in the radial direction, or the time of flight

$$\Omega_r(r, l) = \frac{2\pi\tau}{T} = \pm\frac{2\pi}{T}\int_{r_-}^{r}\frac{dr}{v_r(r,l)} \quad (4)$$

where $T = 2\int_{r_-}^{r_+} dr/v_r(r,l)$ is the period of the radial motion, and $r_\pm$ are the distances of minimum and maximum approaches. From Eq. (3), it is evident that a uniform distribution in $\Omega_r(r)$ is equivalent to the microcanonical ensemble. The difficult part of the calculation is to obtain the direction of the rotational velocity as a function of the angles α, θ, and ϕ. The initial position of an
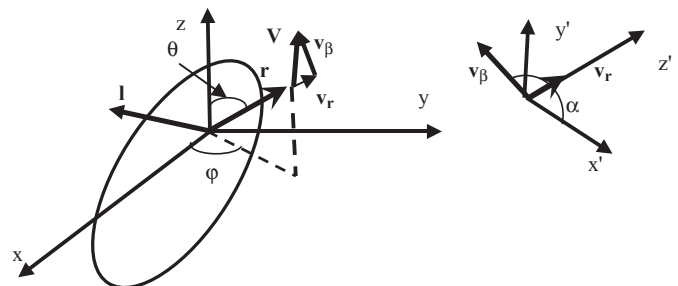

Fig. 1. Schematic of electron trajectory and definition of angles (θ,ϕ,α).

electron is given by

$$\mathbf{r} = \begin{pmatrix} x \\ y \\ z \end{pmatrix} = r \begin{pmatrix} \sin\theta\cos\varphi \\ \sin\theta\sin\varphi \\ \cos\theta \end{pmatrix}.$$

The spherical coordinates can be represented as two rotations of the initial vector pointing along the z-axis, first along the y-axis by the angle θ, and then along the new z-axis by the angle φ. That is, we express

$$\begin{pmatrix} \sin\theta\cos\varphi \\ \sin\theta\sin\varphi \\ \cos\theta \end{pmatrix} = \begin{pmatrix} \cos\varphi & -\sin\varphi & 0 \\ \sin\varphi & \cos\varphi & 0 \\ 0 & 0 & 1 \end{pmatrix} \begin{pmatrix} \cos\theta & 0 & \sin\theta \\ 0 & 1 & 0 \\ -\sin\theta & 0 & \cos\theta \end{pmatrix} \begin{pmatrix} 0 \\ 0 \\ 1 \end{pmatrix}.$$

Correspondingly, the velocity vector is transformed by the same two rotations, from

$$\mathbf{v} = \begin{pmatrix} \cos\varphi & -\sin\varphi & 0 \\ \sin\varphi & \cos\varphi & 0 \\ 0 & 0 & 1 \end{pmatrix} \begin{pmatrix} \cos\theta & 0 & \sin\theta \\ 0 & 1 & 0 \\ -\sin\theta & 0 & \cos\theta \end{pmatrix} \begin{pmatrix} v_\beta\cos\alpha \\ v_\beta\sin\alpha \\ v_r \end{pmatrix} \quad (5)$$

to

$$\mathbf{v} = \begin{pmatrix} v_x \\ v_y \\ v_z \end{pmatrix} = \begin{pmatrix} v_r\sin\theta\cos\varphi + v_\beta(\cos\varphi\cos\theta\cos\alpha - \sin\varphi\sin\alpha) \\ v_r\sin\theta\sin\varphi + v_\beta(\sin\varphi\cos\theta\cos\alpha + \cos\varphi\sin\alpha) \\ v_r\cos\theta - v_\beta\sin\theta\cos\alpha \end{pmatrix}. \quad (6)$$

Note that α is the angle between the x'-axis ($\cos\varphi\cos\theta$, $\sin\varphi\cos\theta$, $-\sin\theta$) and $\mathbf{v}_\beta$, and $\mathbf{r}$ corresponds to the z'-axis.

It is instructive to compare the energy and radial distribution functions obtained from the microcanonical ensemble and quantum mechanics. The radial distribution function in the microcanonical ensemble is bounded by turning points, whereas the quantum mechanical distribution function for a hydrogen-like ion is a Gaussian. Making use of Eq. (3), the energy distribution function, or the distribution function over absolute values of the electron velocity for the Coulomb potential is given by

$$f(v_e, l) = \frac{8v_{nl}^3 v_e}{\pi(v_e^2 + v_{nl}^2)^2 \sqrt{4v_e^2 - L^2(v_e^2 + v_{nl}^2)^2}} \quad (7)$$

where $v_{nl} = \sqrt{2I_{nl}/m}$. The quantum mechanical distribution function over velocity is given by [1,30]

$$f_{qm}(v_e, l) = \frac{32v_{nl}^5 v_e^2}{\pi(v_e^2 + v_{nl}^2)^4}. \quad (8)$$

Eq. (7) gives a much larger distribution than Eq. (8) near the turning points where the electrons move slowly, corresponding to $v \approx Lv_{nl}/2$, and $v \approx 2/L$ for $L \ll 2$. This difference reflects the fact that in quantum mechanics the electrons can tunnel into classically forbidden regions. In principle, it is possible to exactly match the atomic EVDF in classical mechanics to the quantum-mechanical result by choosing an appropriate distribution for the angular momentum $g(L)$ instead of the delta function, $\delta(L-l-0.5)$. For example, completely ignoring any restrictions on momentum incidentally gives the same EVDF as Eq. (8) [1]. However, utilizing the function $g(L)$ is rather artificial, and cannot match both the radial and velocity distribution functions simultaneously. Therefore, we use only the microcanonical ensemble given by Eq. (3), and $L = l+0.5$. Simulations with a different value of angular momentum, e.g., $L = l$, give very similar results (less than 10% difference) for the total cross-section, and are well within the error bars of the method.

Classical trajectory calculation computes an electron trajectory in an atom when another ion or atom with velocity V is passing by at a certain impact parameter, ρ. For calculation of the total cross-section, it is necessary to determine finite result of collision: electron velocity and distance to the target and projectile nuclei at large enough times, when the distance between the projectile and target nuclei is sufficiently large compared with the atom size. There are three possible outcomes: the electron remains close to one of the nuclei or it moves far away from both of them. If the electron kinetic energy (in the appropriate reference frame) is smaller than the attractive potential of the remainder of the target atom or projectile ion, the electron is assumed to be trapped by the respective nuclei, e.g., if

$$\frac{mv^2}{2} < U_T(r)$$

then the electron remains near the target atom, and no ionization or charge-exchange events occur. However, if

$$\frac{m(v - V)^2}{2} < U_P(r)$$

then the electron is trapped by the projectile nucleus, i.e., the charge-exchange event occurs. If the electron is far away from both the target atom and projectile ion then both the conditions

$$\frac{mv^2}{2} > U_T(r) \quad \text{and} \quad \frac{m(v - V)^2}{2} > U_P(r)$$

are satisfied, and the ionization event occurs. The results have to be averaged over all possible initial electron positions. Thus, using the CTMC approach, the ionization, σ_{iz}, or charge exchange, σ_{cx}, cross-sections are given by

$$\sigma^{iz,cx} = \frac{2\pi\rho_{max}\Sigma_{i,j,k,m,s}\rho_i c_{i,j,k,m,s}^{iz,cx}}{N_t} \quad (9)$$

where ρ_i is the impact parameter, ρ_{max} is the maximum impact parameter used in the simulations, and i, j, k, m, s are indexes labeling the simulation in impact parameter, radius, and three spherical angels (θ, ϕ, α); $N_t = N_i N_j N_k N_m N_s$ is the total number of trajectories that are simulated, and $c_{i,j,k,m,s} = 1$, if the ionization/charge-exchange event takes place for calculation of the ionization/charge-exchange cross-section, and $c_{i,j,k,m,s} = 0$, otherwise.
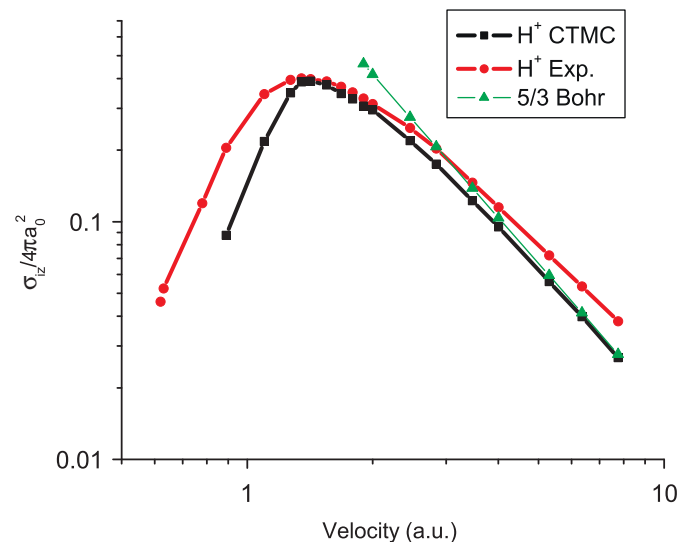
Fig. 2. Normalized ionization cross-section for proton collisions with atomic hydrogen in atomic units; the value of the cross-section is normalized to $4\pi a_0^2 = 3.517 \times 10^{-16}\,\text{cm}^{-2}$; the velocity in atomic units can be calculated from the projectile energy per unit mass from v (a.u.) $= 0.2\sqrt{E\,\text{keV/amu}}$ [1].

3. Comparison of CTMC calculations and experimental data

Using a classical trajectory simulation, we have calculated the ionization and charge-exchange cross-sections for collisions of various ion projectiles with hydrogen and helium targets. Figs. 2–4 show the charge-changing cross-sections (ionization or charge exchange) for fully or partially stripped ions colliding with atomic hydrogen.

3.1. Comparison of CTMC calculations and experimental data for hydrogen target

Atomic units are used in all figures. The experimental data are taken from Ref. [22–25].

At large velocities the CTMC cross-section should approach 5/3 of the Bohr formula [1], i.e.,

$$\sigma = \frac{5}{3}\sigma^{Bohr} = \frac{10\pi a_0^2 v_0^2 E_0 Z_p^2}{3v^2 I_{nl}} \tag{10}$$

where $a_0 = \hbar^2/me^2 = 0.529 \times 10^{-8}$ cm, the velocity is normalized to $v_0 = e^2/\hbar = 2.19 \times 10^8$ cm/s, and the energy is normalized to $E_0 = mv_0^2 = 2Ry = 27.2$ eV, where Ry is the Rydberg energy. The normalizing coefficients are kept in all equations for robust application of the formulae. For efficient manipulation of the formulae, it is worth noting that the normalized projectile ion velocity is v (a.u.) $= 0.2\sqrt{E \text{ keV/amu}}$, where E is the energy per nucleon in keV/amu. Therefore, 25 keV/amu corresponds to the atomic velocity scale.

It should be pointed out that the experimental values for the cross-sections tend to the Bethe limit for $v \gg v_{nl}$ [1], i.e., to

$$\sigma = \frac{2\pi a_0^2 v_0^2 E_0 Z_p^2}{v^2 I_{nl}}\left[0.566\ln\left(v/v_{nl}\right) + 1.26\right] \tag{11}$$

which gives a slightly higher value for the cross-section than the CTMC method.

In carrying out the CTMC calculations it is important to choose reasonable parameters for the simulation to avoid unnecessarily long simulations, and to check convergence over all parameters used in the simulations. These parameters include the initial separation distance between the nuclei of the target and projectile, the maximum impact radius, and the number of simulations. We can sample the initial velocity either randomly or regularly. This does not make a difference for most calculations unless the probability of a process is very rare. A stochastic method for choosing the initial coordinates was used for most simulations, using 100,000–150,000 trajectories. The maximum values of the impact parameter for He, Li, C, and O projectiles were 5.7, 6.5, 11, and 12 au, respectively. For most runs with hydrogen targets, we used an initial separation distance between the nuclei of the target and projectile of 25 a.u. For larger ions, such as oxygen and carbon, this distance increased further for simulations at lower projectile velocities because, due to the larger projectile charge, the projectile can start attracting electrons from atomic hydrogen from a larger distance. The ionization process is rare at low velocities, and only a few special initial conditions contribute to the process. Therefore, these cross-sections are difficult to simulate, e.g., see Ref. [1] for a more detailed description of the ionization process at lower velocity.

The simulation results typically underestimate the experimental data. This is mainly due to the contribution of classically forbidden transitions, which can occur in quantum mechanics. However, the CTMC results and the experimental data curves peak at around the same value of the projectile velocity. For velocities between 1.3 and 2.3 a.u., the simulations appear to provide a good approximation to the experimental values, within 10% for the proton on hydrogen case, see Fig. 2.
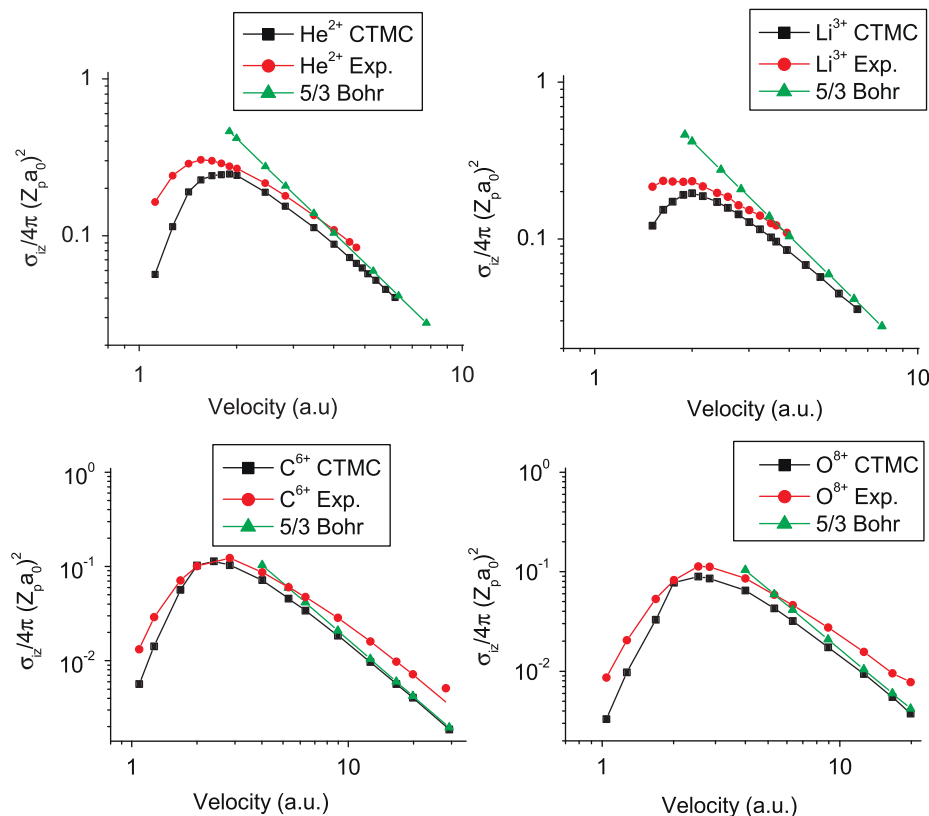
Fig. 3. Normalized ionization cross-sections for fully stripped ions colliding with atomic hydrogen; the value of the cross-section is normalized to $4\pi a_0^2 Z_p^2 = Z_p^2$ 3.517×10^{-16} cm^{-2}. The experimental results for He, Li, and C and O are from Refs. [23,24] and [25], respectively.
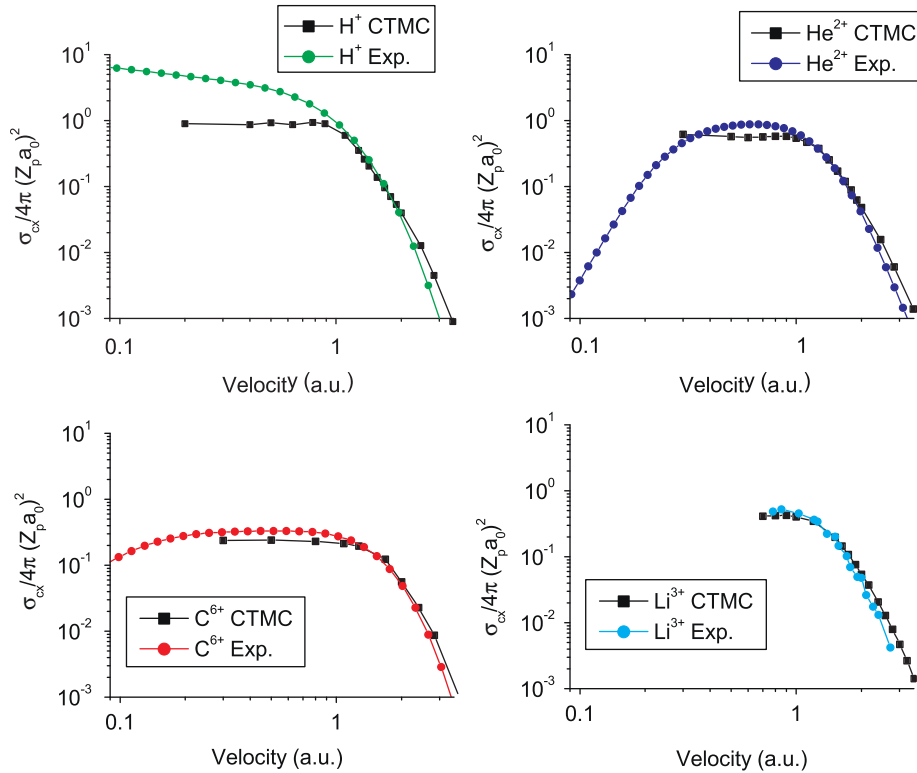
Fig. 4. Normalized charge-exchange cross-sections for collisions of fully stripped ions with atomic hydrogen. The experimental results are from Ref. [23] for H and He, Ref. [24] for Li, and Ref. [25] for C.

For charge-exchange cross-sections, the CTMC method predicts reasonably well the value of the cross-section for projectile velocity in the range $v \in [0.9, 3]$. At smaller velocities, there are important quantum-mechanical effects which lead to much larger cross-sections for collisions where the projectile is identical to the target nucleus, or much smaller cross-sections for other projectiles, as evident from Fig. 4.

We have also simulated cross-sections for more complex projectile ions, Ar^{+3} and Ar^{+7}. The ion potential was obtained from a modified (for ions) Thomas–Fermi theory [22]. In normalized atomic units, the potential is given by

$$V_p(r) = \begin{cases} \dfrac{Z}{r}K_s\left(\dfrac{rZ^{\frac{1}{3}}}{b}\right) + \dfrac{Z_p}{R_{ion}} & \text{if } r < R_{ion} \\[2mm] \dfrac{Z_p}{r} & \text{if } r \geqslant R_{ion} \end{cases} \quad (12)$$

where

$$K_s(x) = \left[1 - \left(\frac{x}{S_1}\right)^3\right] \cdot \frac{1}{(1 + 0.02747\sqrt{x} + 1.243x - 0.1486x^{1.5} + 0.2302x^2)}$$

is an approximation to the Thomas–Fermi potential, and $b = 0.8853$, $Z = 18$ (argon nucleus charge), and $S_1 = 3.96175$ is obtained from the Thomas–Fermi model to match the asymptotic behavior of the ion potential at large radius $R_{ion} = bS_1/Z^{1/3} = 1.3383$.

In Fig. 5 the normalized values of cross-sections of Ar^{+3} and Ar^{+7} ions are plotted against the projectile velocity and compared with the experimental data [26] and the previous results for H^+ and Li^{+3} ions. For the most part the two Ar ion cross-sections resemble the others in their basic shape and curvature. For instance, note the similarities between Li^{+3} and Ar^{+3}. However, also note that the CTMC results for Ar^{+3} cross-sections do not approach the 5/3 Bohr limit at high velocities unlike those of other ions. This is because of the large contribution to ionization for impact parameters inside the
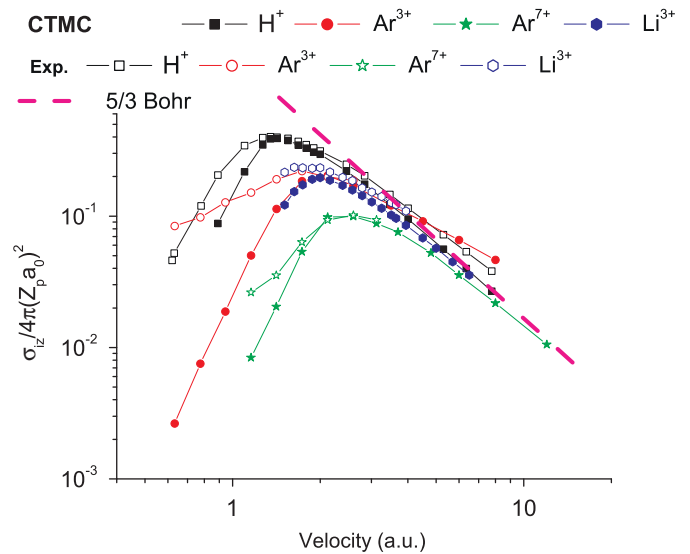
Fig. 5. Ionization cross-sections of argon ions (Ar^{+3} and Ar^{+7}) compared with fully stripped ions of the same charge (H^+ and Li^{+3}) on atomic hydrogen. The experimental values for Ar ions are taken from Ref. [26].

ion radius, $\rho < R_{ion}$, where much larger forces act on the electron than just the Coulomb force, Z_p/r^2. Fig. 6 shows a comparison with available experimental data for charge-exchange cross-sections for collisions of argon ions (Ar^{+3}) with hydrogen.

3.2. Comparison of CTMC calculations and experimental data for helium target

Similar simulations have been performed for helium. In this case, we used a simple approximation for the potential acting on

an electron inside the helium atom taken from Ref. [27], and normalized atomic units is given by

$$V_t(r) = (r\beta + 1)\frac{(\zeta e^{-2r\beta})}{2r} + \frac{1}{r} \qquad (13)$$

where $\beta = 1.65$ and $\zeta = 2$. The ionization potential for neutral He is $24.59\,eV = 0.904\,a.u.$ Since there are two electrons that can be ionized, we calculate the total cross-sections for one electron and then multiply it by a factor of two (independent electron approximation). The results are shown in Fig. 7. The experimental values were taken from [28].

3.3. Comparison of CTMC calculations and experimental data for potassium projectile

The cross-sections for charge-changing collisions of fast potassium ions with different target atoms are needed to estimate the generation of electrons in the accelerator section of ion beams in the High-Current Experiment (HCX) and the Neutralized Drift Compression Experiment (NDCX) at Lawrence Berkeley National Laboratory (LBNL) [2,10]. Therefore, these total cross-sections have been measured in Ref. [29]. The sum of ionization and charge-exchange cross-sections for several gas targets (H$_2$, N$_2$, He, Ne, Kr, Xe, Ar, and water vapor) impacted by a 1 MeV K$^+$ beam

were measured. In a high-current ion beam, the self-electric field of the beam is high enough that the ions produced from gas ionization or charge exchange by the ion beam are quickly swept aside in the accelerator. The flux of expelled ions is measured by a retarding field analyzer. This allowed accurate measurements of the total charge-changing cross-sections (ionization plus charge exchange) of the beam interacting with gas. The cross-sections for H$_2$, He, and N$_2$ have been simulated using the CTMC method and compared with experimental results, showing a very good agreement.

Fig. 8 shows the CTMC theoretical prediction for charge-changing cross-sections as a function of the projectile energy. In the low-energy region, i.e., when the projectile velocity is much slower than the least tightly bound electron in the target molecule, the charge-exchange process dominates over ionization. When the projectile velocity becomes much larger than the velocity of the least tightly bound electron in the target atom, the charge-exchange cross-section decreases rapidly [30]. The ionization cross-section decreases with increasing projectile energy, approaching for large energies, the $(\ln E)/E$ dependence of the Bethe formula (11) [1]. Therefore, in the high-energy region, i.e., when the projectile velocity is much larger than the least tightly bound electron in the target molecule, ionization
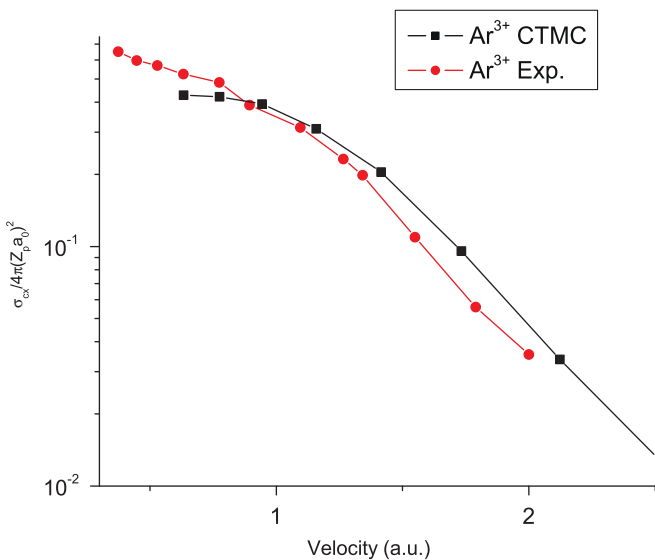

Fig. 6. Charge-exchange cross-sections for collisions of argon ions (Ar^{+3}) with atomic hydrogen. The experimental values were taken from Ref. [26].
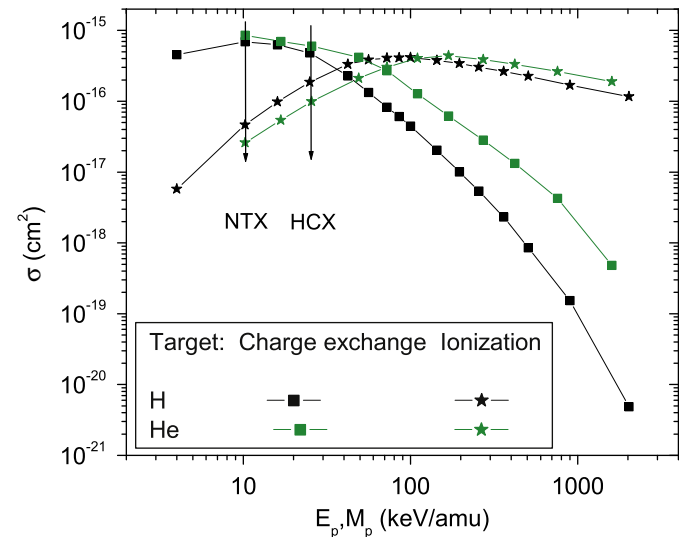

Fig. 8. Charge-exchange cross-sections and ionization cross-sections of atomic H and He target ions interacting with K$^+$ ions, predicted using CTMC calculations. The HCX parameters (1 MeV K$^+$ ion) correspond to 25 keV/amu.
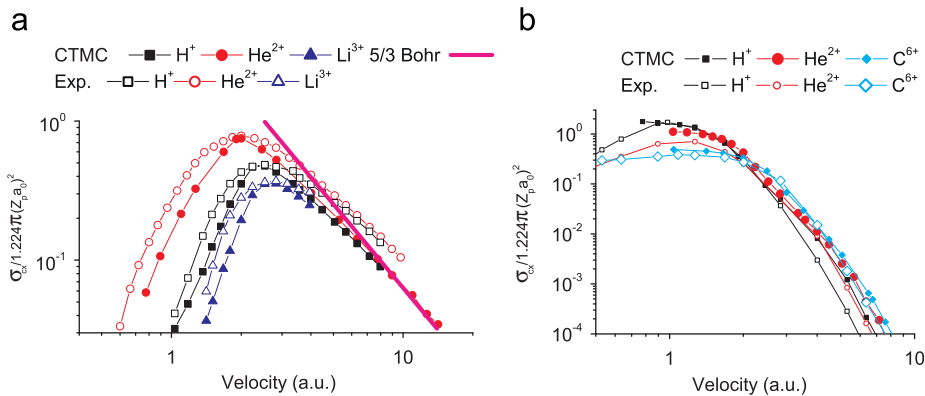

Fig. 7. Charge-changing cross-sections for fully stripped ions on helium corresponding to: (a) ionization, and (b) charge exchange. The experimental values were taken from [28]. The value of the cross-section is normalized to $\pi a_0^2(Z_p E_0/I_{nl})^2 = 1.224\pi Z_p^2 a_0^2 = 0.719 \times 10^{-16}Z_p^2\,cm^{-2}$; the projectile velocity in atomic units can be calculated from the projectile energy per unit mass from $v\,(a.u.) = 0.2\sqrt{E}$ keV/amu [1].
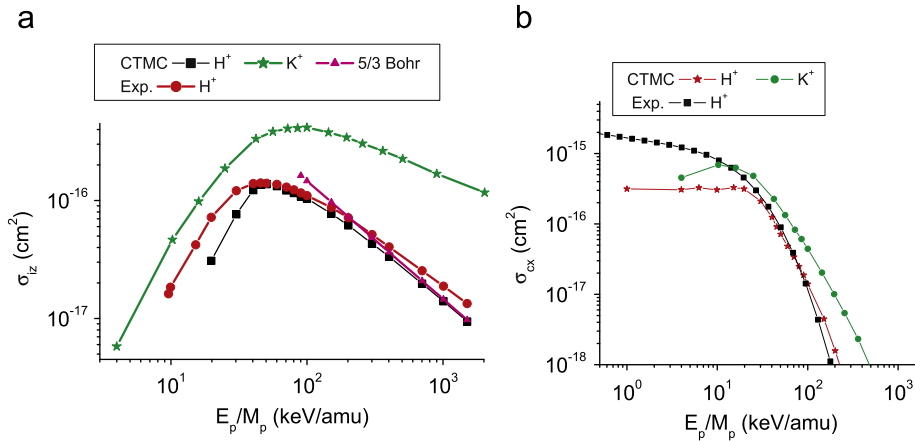
Fig. 9. Comparison of ionization cross-section (a), and (b) charge-exchange cross-sections for proton and potassium ion projectiles colliding with atomic hydrogen. The experimental data are from Refs. [1,3].

dominates over the charge-exchange mechanism and has a larger cross-section.

Fig. 9 illustrates that the contribution of collisions with impact parameter less than potassium ion radius (inside the potassium ion) is important for cross-sections estimates, because the potassium ion cross-sections are significantly larger than the proton cross-sections. This difference is much larger than the difference for argon ions, shown in Fig. 6. Therefore, it is important to accurately model the potassium ion atomic potential near the outer edge of the ion radius. The atomic potential of potassium ion can be determined either by Thomas–Fermi theory or Hartree–Fock theory, which include orbital effects.

The Thomas–Fermi distribution of the electron density, n_e, in atomic units as a function of the potential, ϕ, is given by [22]

$$n_e = \frac{1}{3\pi^2}[2(\phi - \phi_0)]^{3/2} \tag{14}$$

and the potential is determined from the Poisson equation

$$\nabla^2 \phi = \frac{8\sqrt{2}}{3\pi}(\phi - \phi_0)^{3/2}. \tag{15}$$

The constant ϕ_0 has to be determined from the condition at the ion radius $r = r_0$, where $\phi = \phi_0$ and the electron density becomes zero. Because there are no electrons beyond the ion radius, the potential at this point should be $\phi(r) = z_{ion}/r$, which gives $\phi_0 = z_{ion}/r_0$. The values of r_0, ϕ_0 are obtained numerically. For a potassium ion K$^+$, it follows that $z_{ion} = 1$, $Z = 19$, and the ion radius is $r_0 = 5.22$ a.u.

The Hartree–Fock atomic wave equations are solved using Slater determinants [20]. An electron orbital wave function with quantum numbers (n,l,m) are represented as a linear combination of the Slater functions [31]

$$\chi_{n,l,m}(\mathbf{r}) = \sum_p \beta_p \frac{(2\alpha_p)^{n_p+1/2}}{[(2n_p)!]^{1/2}} r^{n_p-1} e^{-\alpha_p r} Y_{l,m}(\phi, \theta) \tag{16}$$

where β_p and α_p are the variational parameters of the pth expansion coefficients of Hartree–Fock function, n_p is the principal number of the electron orbital in the decomposition, and $Y_{l,m}$ represents the spherical harmonic, which is dependent on the angular momentum, l, and magnetic moment, m. The radial electron density can be calculated from the electron wave
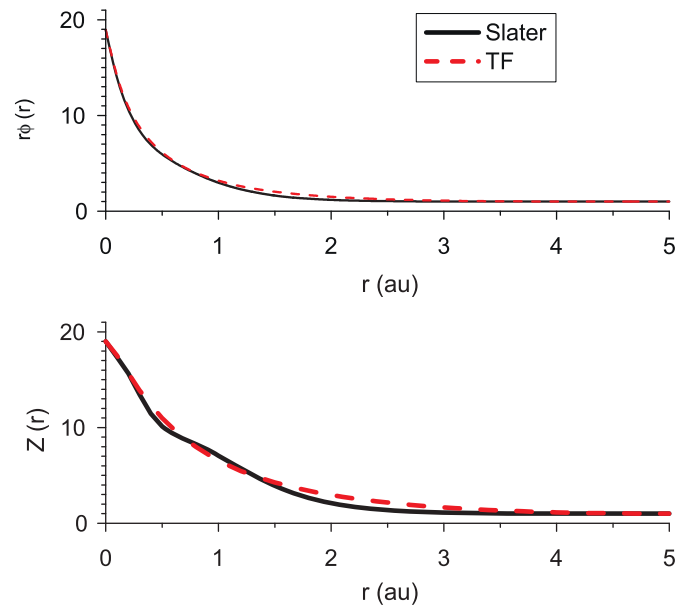
Fig. 10. Comparison of Thomas–Fermi and Slater models for the potassium ion potential, $r\phi(r)$, and profile of charge, $Z(r)$, inside a sphere of radius r. Note the differences between the two models at the outer edge of the ion. The orbital structure is evident for the Slater model.

function in Eq. (16), averaging over angles, which gives

$$\rho_{n,l}(r) = \left\{ \sum_p \beta_p \frac{(2\alpha_p)^{n_p+1/2}}{[(2n_p)!]^{1/2}} r^{n_p-1} e^{-\alpha_p r} \right\}^2. \tag{17}$$

In Eq. (17), the normalization condition is $\int_0^\infty \rho_{n,l}(r)r^2 dr = 1$. The potential is determined from the Poisson equation with $n_e(r) = \sum_{n,l} \rho_{n,l}(r)$, which can be expressed in atomic units as

$$\phi(r) = \frac{Z}{r} - \frac{\int_0^r \sum_{n,l} \rho_{n,l}(r')r'^2 \, dr'}{r} - \int_r^\infty \sum_{n,l} \rho_{n,l}(r')r' \, dr'. \tag{18}$$

Here, the orbital contributions to the electron density, $\rho_{n,l}(r)$, are given by Eq. (17). Taking the derivative of the potential gives the electric field

$$E(r) = \frac{Z(r)}{r^2} \tag{19}$$

Table 1

Ionization and charge-exchange cross-sections for the interaction of 1 MeV K^+ with H_2, He, and Ne.

Gas	Charge exchange cross-section (10^{-16} cm^2)		Ionization cross-section (10^{-16} cm^2)	
	Slater	TF	Slater	TF
H_2	5.92	9.68	3.00	3.74
He	4.10	5.98	1.10	0.994
Ne	9.46		3.91	

TF denotes the calculation using Thomas–Fermi model of potassium ion, and Slater indicates the more accurate model given by Eq. (18).

Table 2

Comparison of the calculated values of the total cross-sections (sum of the ionization and charge exchange cross-sections) with the experimental data [29] for the interaction of 1 MeV K^+ with H_2, He, and Ne.

Gas	Experiment (10^{-16} cm^2)	CTMC, Slater model (10^{-16} cm^2)
H_2	13.5 ± 1.5	8.9
He	5.62 ± 0.57	5.20
Ne	11.9 ± 1.0	13.4

where $Z(r) = Z - \int_0^r \sum_{n,l} \rho_{n,l}(r') r'^2 \, dr'$ is the total charge inside a sphere of radius r.

Calculations show that Thomas–Fermi theory does not describe accurately the ion potential at the outer edge of the potassium ion, even though the potassium nucleus has relatively high charge Z ($Z = 19$), and the Thomas–Fermi model describes well most of the potential, as shown in Fig. 10. In contrast to the highly charged argon ions in Fig. 5, the difference in atomic potentials for singly charged potassium ions is more important, and gives an error of about 20% compared with the calculations utilizing more accurate Slater model in Ref. [20] as shown in Table 1.

The results of simulations using the CTMC method for the ionization and charge-exchange cross-sections for the interaction of 1 MeV K^+ with H_2, He, and Ne are summarized in Table 1. For a 1 MeV K^+ beam, the values of the charge-exchange cross-sections are 2–4 times higher than the ionization cross-sections; the total cross-section agrees well with the experimental data [29], as shown in Table 2.

4. Challenges in CTMC calculations of multielectron events

We have attempted to simulate multielectron target or projectile ions classically by taking into account several electrons simultaneously, similar to previous calculation where only the single electron trajectory was simulated. As a first step, simulations of a helium atom have been performed. However, the problem with simulations using the CTMC approach for multielectron atoms or ions is that in classical mechanics multielectron atoms are not stable, for example, the simplest helium atom has very few stable electron trajectories [32]. Classically, the two helium electrons are allowed to exchange energy, so that for practically all initial conditions corresponding to the ground state of the helium atom, one electron drops down to a lower orbit with a smaller energy, and the other electron acquires enough energy to escape to infinity from the nucleus, and the atom auto-ionizes itself even without interaction with the projectile. Quantum mechanically, this cannot occur if the system is in its ground state.

In order to avoid artificial auto-ionization in classical mechanics, we can modify the electron repulsion force between two electrons to reduce the energy exchange between them at close collisions, for example, the force can be modified to $F(r) =$
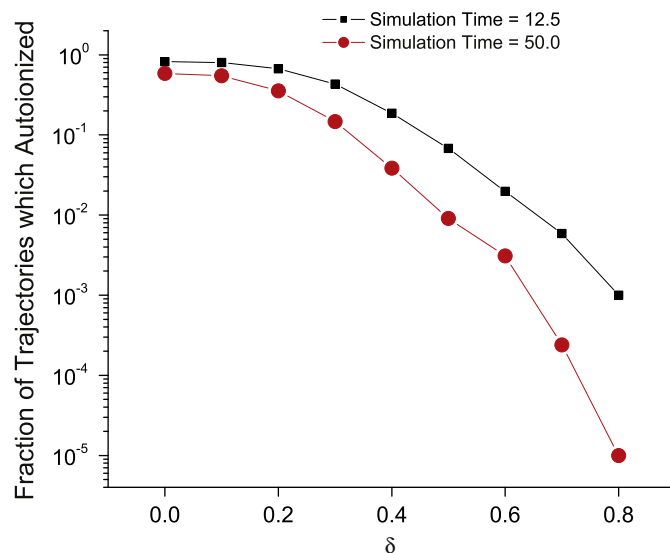
Fig. 11. Fraction of auto-ionizing two-electron helium atom orbits for two simulation time intervals.

$-r/(r^2 + \delta^2)^{3/2}$, where δ is a constant of order unity in atomic units. Fig. 10 shows the results of simulation runs for different values of δ and different simulation time intervals. The most typical time intervals for cross-section simulations are between 12.5 and 50.0 a.u. Therefore, Fig. 11 shows approximate upper and lower bounds on stable orbits. Each point on the graph represents 10,000 trajectories, except for the $\delta = 0.7$ and 0.8 points on the curve for simulation time = 50.0, which used 100,000 trajectories. The number of orbits in which auto-ionization occurred was recorded and expressed as a fraction of the total trajectories simulated. Fig. 10 shows that for typical simulation time scales, the addition of δ term in the electron repulsion force term is an effective way to decrease the number of trajectories which auto-ionize. However, an effective algorithm needs to be developed to make sure that artificial auto-ionization does not contribute to the charge-changing collisions.

5. Conclusions

As evident from figures showing comparisons between the simulations and experimental data, the CTMC simulations match the experimental results for projectile velocities between 1 and 3 atomic units, which correspond to the region near the maximum value of the cross-section. The CTMC method can underestimate the value of cross-sections outside this velocity range. An effective algorithm needs to be developed to make sure that artificial auto-ionization in collisions of two electrons in classical mechanics does not contribute to charge-changing collisions.

Acknowledgments

References

[1] I.D. Kaganovich, E.A. Startsev, R.C. Davidson, New J. Phys. 8 (2006) 278.
[2] B.G. Logan, et al., Nucl. Instr. and Meth. A 577 (2007) 1.
[3] H.-D. Betz, Rev. Mod. Phys. 44 (1972) 465.
[4] H. Beyer, V.P. Shevelko, Atomic Physics with Heavy Ions, Springer, Berlin, 1999.
[5] R.A. Bosch, Phys. Rev. ST Accel. Beams 6 (2003) 074201.
[6] A. Smolyakov, W. Fischer, C. Omet, P. Spiller, GSI Report no. GSI-Acc-Report-2005-11-001, 2005.
[7] W. Fischer, M. Bai, J.M. Brennan, M. Blaskiewicz, P. Cameron, H.C. Hseuh, H. Huang, W. MacKay, T. Roser, T. Satogata, L.A. Smart, D. Trbojevic, S.Y. Zhang, Proceedings of the European Particle Accelerator Conference, Paris, France, 2002, p. 1485.
[8] T. Demma, S. Petracca, F. Ruggiero, G. Rumolo, F. Zimmermann, Phys. Rev. ST Accel. Beams 10 (2007) 114401.
[9] L. Wang, F. Zimmermann, SLAC Report no. SLAC-PUB-12642, 2007.
[10] P.K. Roy, S.S. Yu, E. Henestroza, et al., Phys. Rev. Lett. 95 (2005) 234801.
[11] R.E. Olson, R.L. Watson, V. Horvat, K.E. Zaharakis, J. Phys. B 35 (2002) 1893; R.E. Olson, R.L. Watson, V. Horvat, A.N. Perumal, Y. Peng, Th. Stöhlker, J. Phys. B: At. Mol. Phys. 37 (2004) 4539.
[12] R.L. Watson, Y. Peng, V. Horvat, G.J. Kim, R.E. Olson, Phys. Rev. A 67 (2003) 022706.
[13] R.D. Dubois, A.C.F. Santos, Th. Stöhlker, F. Bosch, A. Bräuning-Demian, A. Gumberidze, S. Hagmann, C. Kozhuharov, R. Mann, A. Oršić Muthig, U. Spillmann, S. Tachenov, W. Bart, L. Dahl, B. Franzke, J. Glatz, L. Gröning, S. Richter, D. Wilms, K. Ullmann, O. Jagutzki, Phys. Rev. A 70 (2004) 032712.
[14] D. Mueller, L. Grisham, I.D. Kaganovich, R.L. Watson, V. Horvat, K.E. Zaharakis, Phys. Plasmas 8 (2001) 1753.
[15] D. Mueller, L. Grisham, I. Kaganovich, R.L. Watson, V. Horvat, K.E. Zaharakis, Y. Peng, Laser Part. Beams 20 (2002) 551.
[16] A.C.F. Santos, R.D. DuBois, Phys. Rev. A 69 (2004) 042709.
[17] R.E. Olson, R.L. Watson, V. Horvat, K.E. Zaharakis, Phys. Rev. A 67 (2003) 022706.
[18] G. Schiwietz, W. Fritsch, J. Phys. B: At. Mol. Phys. 20 (1987) 5463.
[19] R. Abrines, I.C. Percival, Proc. Phys. Soc. 88 (1966) 861.
[20] E. Clementi, C. Roetti, At. .Data Nucl. Data Tables 14 (1974) 177.
[21] I.D. Kaganovich, et al., Nucl. Instr. and Meth. A 544 (2005) 91.
[22] L.D. Landau, E.M. Lifshitz, Quantum Mechanics: Non-Relativistic Theory, Butterworth-Heinemann, Oxford, Burlington, MA, 2003.
[23] C.F. Barnett, (Ed.), Atomic Data for Fusion, vol. 1, Collisions of H, H2, He, and Li Atoms and Ions with Atoms and Molecules, vol. 1, ORNL-6086, 1990.
[24] M.B. Shah, et al., J. Phys. B: At. Mol. Phys. 11 (1978) 121.
[25] R.A. Phaneuf, et al. (Eds.), Atomic Data for Fusion, vol. 5, Collisions of Carbon and Oxygen Ions with Electrons, H, H2, and He, ORNL-6090, 1987.
[26] M.B. Shah, H.B. Gilbody, J. Phys. B: At. Mol. Phys. 16 (1983) 4395.
[27] V.P. Shevelko, I. Yu. Tolstikhina, Th. Stoehlker, Nucl. Instr. and Meth. B 184 (2001) 295.
[28] M.B. Shah, H.B. Gilbody, J. Phys. B: Mol. Phys. 18 (1985) 899; M.B. Shah, P.M. Callion, H.B. Gilbody, J. Phys. B: Mol. Phys. 22 (1989) 3037.
[29] M. Kireeff Covo, I.D. Kaganovich, A. Shnidman, A.W. Molvik, J.L. Vujic, Phys. Rev. A 78 (2008) 032709.
[30] R.K. Janev, L.P. Presnyakov, V.P. Shevelko, Physics of Highly Charged Ions, Springer, Berlin, 1985.
[31] J.C. Slater, Phys. Rev. 98 (1955) 4.
[32] T. Yamamoto, K. Kaneko, Phys. Rev. Lett. 70 (1993) 1928.